mater.scichina.com link.springer.com

Published online 8 September 2023 | https://doi.org/10.1007/s40843-023-2540-9
Sci China Mater 2023, 66(10): 4012–4021

Controlled length and number of thermal conduction pathways for copper wire/poly(lactic acid) composites *via* 3D printing

Tengbo Ma[1†], Kunpeng Ruan[1†], Yongqiang Guo[2*], Yixin Han[1] and Junwei Gu[1*]

ABSTRACT **Thermal conduction pathways play crucial roles in comprehending thermal transport in thermally conductive polymer composites. However, there is a lack of in-depth investigation on how the thermal conduction pathways (length and number) influence the thermal conductivity coefficients (λ) of the composites. In this work, three-dimensional (3D) printing is performed to fabricate the thermally conductive 1D copper wire/poly(lactic acid) (1D-Cw/PLA) composites, allowing for controlling the length and number of Cw thermal conduction pathways. And one thermal conduction model is also proposed and established for polymer composites with 1D thermal conduction pathways, elucidating the quantitative relationship between thermal conduction pathways and thermal conductivity. For composites with the same amount of Cw, the in-plane λ ($\lambda_{//}$) of thermally conductive 1D-Cw/PLA composites is positively correlated with the number and length of Cw thermal conduction pathways. Specifically, when the volume fraction of Cw is 25.1 vol%, the $\lambda_{//}$ of 1D-Cw/PLA composites, containing 20 intact Cw thermal conduction pathways, can reach up to 4.23 W m^{-1} K^{-1}, which is 87.2% higher than that of 1D-Cw/PLA composites without intact Cw thermal conduction pathways (2.26 W m^{-1} K^{-1}), 72.0% higher than that of 1D-Cw/PLA composites with short Cw (2 intact Cw and 18 Cw broken at the half, 2.46 W m^{-1} K^{-1}), and 1527% higher than that of the pure PLA matrix (0.26 W m^{-1} K^{-1}). Furthermore, the predicted λ values from our established thermal conduction model and empirical equation show no significant difference from the measured λ at a 95% confidence level.**

Keywords: 3D printing, thermally conductive composites, thermal conduction

INTRODUCTION

Electronic devices such as mobile phones, computers, and smart machines inevitably generate a significant amount of waste heat during their operation, which would adversely affect their stability, reliability, and service life [1–3]. To address this issue, thermally conductive polymer composites have gained widespread usage in the field of electronics, which can offer the advantage of tunable thermal performance, convenient processing, and cost-effectiveness. By effectively reducing the operating temperature of electronics, the obtained composites can ensure their operational stability [4–6]. Furthermore, the increasing emphasis on high power and integration in the 5G era has placed even greater demands on the thermal conduction of polymer composites [7–9].

Researchers commonly utilize the methods such as solution blending, melt blending, and *in situ* polymerization to incorporate highly thermally conductive fillers (e.g., carbon-based [10–13], metallic [14–17], and ceramic [18–21] fillers) into polymer matrix for the preparation of thermally conductive composites. However, reaching high thermal conductivity often requires a substantial inclusion of thermally conductive fillers, which would lead to poor mechanical and processing properties of the resulting composites [22–24]. Studies have shown that optimizing and controlling the ordered distribution of thermally conductive fillers within polymer matrix and efficiently constructing thermal conduction pathways formed by the overlap of these fillers can yield superior thermal conduction properties at relatively lower filler loadings [25–28]. For instance, Sun *et al.* [29] prepared thermally conductive carbon nanofiber/poly(*L*-lactic acid)/poly(butylene adipate-*co*-terephthalate) (CNF/PLLA/PBAT) composites *via* melt extrusion and stretch technology. With addition of 10 wt% CNF, the thermal conductivity coefficient (λ) of these composites reached 1.53 W m^{-1} K^{-1}, showing a 31.9% enhancement compared with that of CNF/PLLA/PBAT composites prepared *via* conventional hot-pressing method (1.16 W m^{-1} K^{-1}). This improvement was mainly attributed to the shearing effect induced by the process, which led to the more oriented arrangement of CNF within the PLLA/PBAT matrix, facilitating the formation and enhancement of thermal conduction pathways. In our previous work, Ma *et al.* [30] capitalized on the shear effect during the fused deposition modeling (FDM) three-dimensional (3D) printing process to promote the oriented alignment of graphene nanoplatelets (GNPs) inside poly(lactic acid) (PLA) matrix, resulting in the preparation of oriented thermally conductive GNPs/PLA (o-GNPs/PLA) composites. With addition of 20 wt% GNPs, the λ of o-GNPs/PLA composites reached 2.90 W m^{-1} K^{-1}, which was 1.6 times higher than that of randomly dispersed thermally conductive GNPs/PLA composites with the same mass fraction of GNPs (1.82 W m^{-1} K^{-1}).

However, researchers have predominantly focused on the construction of thermal conduction pathways inner polymer

[1] Shaanxi Key Laboratory of Macromolecular Science and Technology, School of Chemistry and Chemical Engineering, Northwestern Polytechnical University, Xi'an 710072, China
[2] School of Chemistry, Beihang University, Beijing 100191, China
[†] These authors contributed equally to this work.
[*] Corresponding authors (emails: gyqnpu@163.com (Guo Y); gjw@nwpu.edu.cn or nwpugjw@163.com (Gu J))

composites and often attribute the enhancement of thermal conductivity solely to the formation and improvement of these pathways [31,32]. It is important to note that there is still a lack of in-depth research on the relationship between the properties of thermal conduction pathways (such as length and number) and the thermal conductivity of polymer composites. In previous studies, researchers have explored the intrinsic relationships between thermal conduction pathways and thermal conductivity by developing thermal conduction models. For example, the Agari thermal conduction model [33,34] considered the difficulty levels of forming thermal conduction pathways through thermally conductive fillers and quantified it as a freedom factor. This model established a simple numerical relationship between thermal conduction pathways and thermal conductivity. The Privalko thermal conduction model [35] proposed that when the amount of conductive filler reached a critical volume fraction, thermal conduction pathways and the polymer matrix interpenetrated each other. This model introduced a stepwise averaging method to express the correlation between thermal conduction pathways and thermal conductivity. However, most thermal conduction models tend to oversimplify the internal factors influencing changes in thermal conductivities for polymer composites and do not establish a quantitative relationship between the properties of thermal conduction pathways and thermal conductivity. As a result, these models encounter difficulties when tasked with directing the optimization and controlled fabrication of thermally conductive polymer composites.

Deciphering the intrinsic relationship between the length and number of thermal conduction pathways and thermal conductivity hinges on the ability to control the design of these pathways. In recent years, 3D printing has emerged as a promising technology that enables precise and controllable design of thermal conduction pathways [36–38]. Gao *et al.* [39] employed FDM 3D printing technology to construct precise thermal conduction pathways using boron nitride nanosheets (BNNSs) inner thermoplastic polyurethane (TPU), resulting in the preparation of thermally conductive BNNSs/TPU composites. The BNNSs/TPU composites exhibited a λ of 1.80 W m^{-1} K^{-1} with 30 wt% BNNS, signifying a striking 650% increase when compared with pure TPU (0.24 W m^{-1} K^{-1}). Guiney *et al.* [40] utilized direct ink writing 3D printing technology to construct controllable hexagonal boron nitride (hBN) thermal conduction pathways inner poly(lactic-*co*-glycolic acid) (PLGA), leading to the preparation of thermally conductive hBN/PLGA composites. At a volume fraction of 40 vol% hBN, the hBN/PLGA composites exhibited a λ of 2.10 W m^{-1} K^{-1}, which was 10 times higher than that of pure PLGA (0.20 W m^{-1} K^{-1}). Although 3D printing technology enables precise construction and controllable distribution of thermal conduction pathways, most studies have primarily focused on utilizing it as a manufacturing process to prepare highly thermally conductive polymer composites. The internal influences of the length and number of thermal conduction pathways on the thermal conductivities of the obtained composites have not received much attention.

In this work, the 3D printing technology is utilized to fabricate PLA bulks with embedded parallel holes, which are subsequently filled with 1D copper wires (1D-Cw) of varying lengths, numbers, and diameters. These Cw act as efficient thermal conduction pathways within PLA matrix. By employing the hot-pressing method, thermally conductive 1D-Cw/PLA composites with controllable lengths and numbers of Cw thermal conduction pathways are obtained. The influences of these parameters on the thermal conductivities of the 1D-Cw/PLA composites are investigated using the Hot Disk thermal constant analyzer. To further characterize and simulate the thermal conduction behavior, infrared thermography and finite element analysis are employed. Additionally, one thermal conduction model is proposed and established, specifically designed for polymer composites featuring 1D thermal conduction pathways. The aim of this work is to elucidate the quantitative relationship between the properties of thermal conduction pathways and the thermal conduction properties of polymer composites.

EXPERIMENTAL SECTION

Preparation of thermally conductive 1D-Cw/PLA composites

PLA powder (Grade: 4032D, Nature Work, USA) was processed into 1.75-mm diameter PLA filaments using a screw extruder (SJ25 type, Zhangjiagang Aoruide Machinery Co., Ltd.). The filament was then loaded into an FDM 3D printer (CreatBot F160 type, Henan Suwei Electronic Technology Co., Ltd.) to fabricate PLA bulks containing 20 parallel holes, following the instruction provided in the ".gcode" file generated by CreatWare V6.5.2 software. Different numbers, lengths, and diameters of pure Cw with diameters of 0.8, 0.6, and 0.4 mm (Suqian Jia'ao Trading Co., Ltd.) were embedded into the PLA holes. Subsequently, the PLA bulks containing Cw were placed in a mold and compressed at 155°C for 10 min to prepare thermally conductive 1D-Cw/PLA composites with dimension of 20 mm × 20 mm × 2 mm. Fig. 1a shows the schematic illustration for preparation of thermally conductive 1D-Cw/PLA composites. The axial direction of the Cw is denoted as the *x*-axis, while the radial direction of the Cw, parallel to the upper surface of the sample, is denoted as the *y*-axis. Fig. 1b presents the schematic illustration for structures of thermally conductive 1D-Cw/PLA composites, and the detailed information is provided in Table S1. In Group 1, all the Cw are intact. In Groups 2–4, the diameters of the Cw are 0.4, 0.6, and 0.8 mm, respectively, and there are 0, 4, 8, 12, and 16 intact Cw in each group. Both Group 5 and Group 6 have only 2 intact Cw, with the remaining 18 Cw in Group 5 broken at the 3/4 position, while the broken position in Group 6 is at the 1/2 position.

Characterizations

The λ values of the thermally conductive 1D-Cw/PLA composites were measured using a thermal constant analyzer (TPS2200, Hot Disk, Sweden) in accordance with the ISO 22007-2:2015 standard. The temperature distribution of the thermally conductive 1D-Cw/PLA composites was captured using an infrared thermal imaging device (Ti 300, Fluke, USA). Additionally, COMSOL Multiphysics software was employed to simulate the thermal conduction behaviors within 1D-Cw/PLA composites.

RESULTS AND DISCUSSION

Number of thermal conduction pathways, the more the better?

Fig. 2a–c depict the in-plane λ ($\lambda_{//}$) of thermally conductive 1D-Cw/PLA composites with different numbers of intact Cw thermal conduction pathways. With the same amount of Cw, the $\lambda_{//}$ of 1D-Cw/PLA composites increases as the number of intact Cw

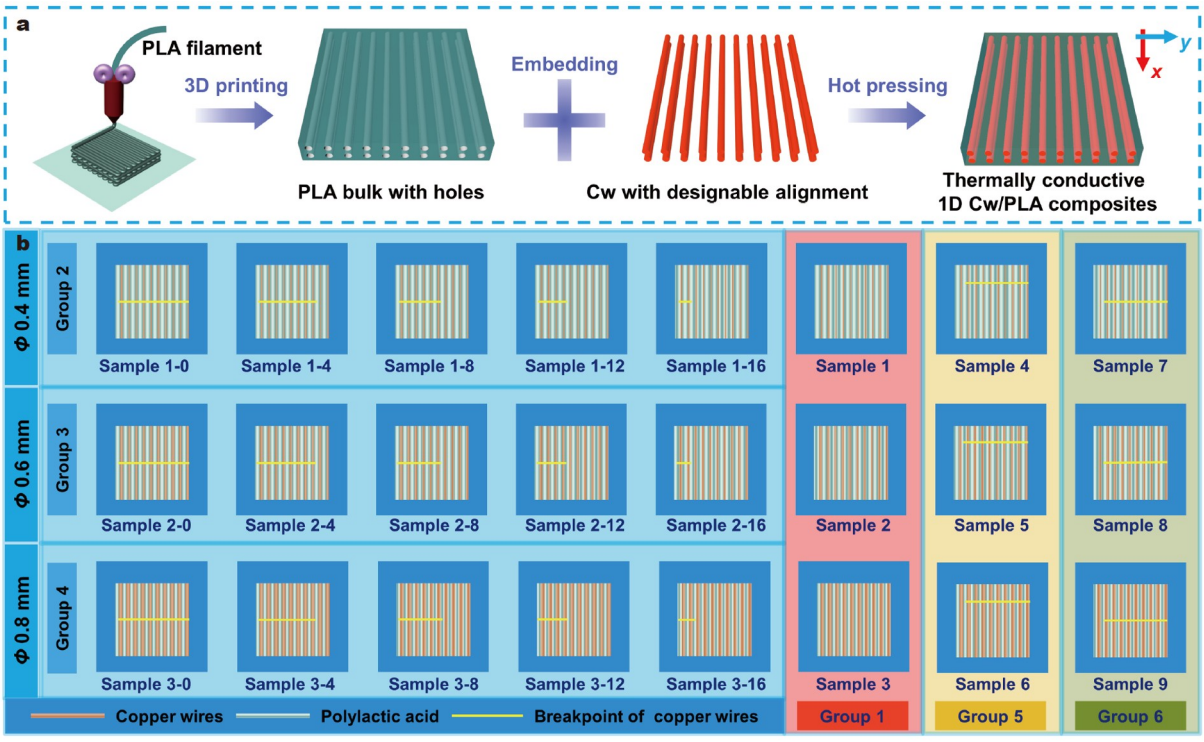

Figure 1 Schematic illustration for the preparation (a) and structures (b) of thermally conductive 1D-Cw/PLA composites.

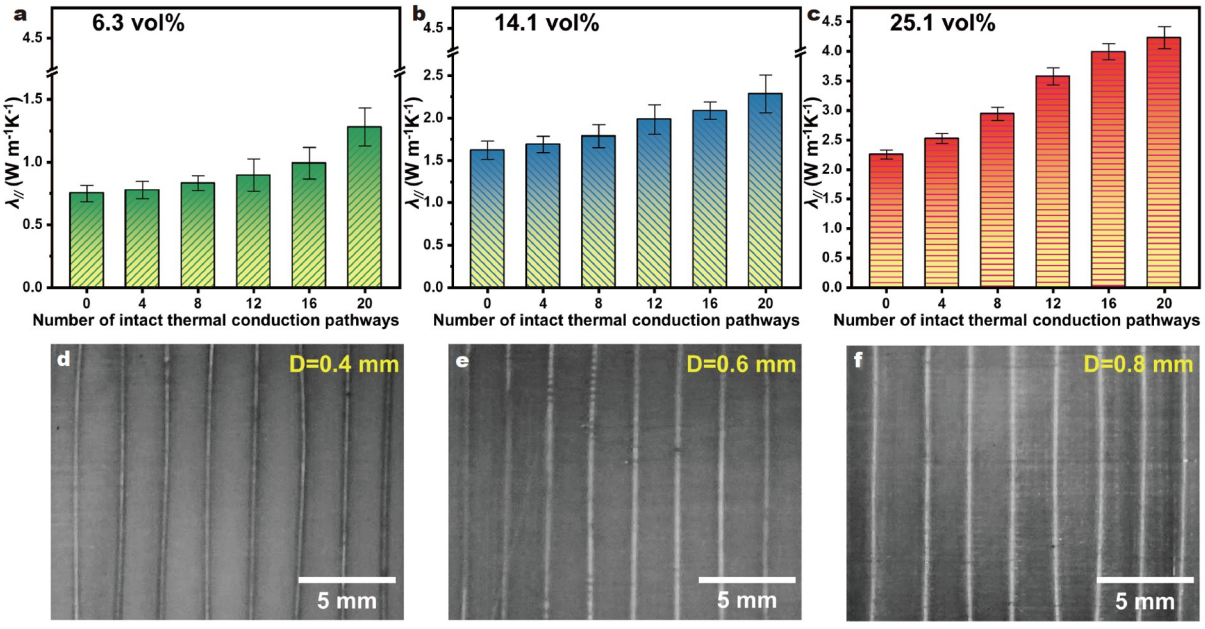

Figure 2 $\lambda_{//}$ of thermally conductive 1D-Cw/PLA composites containing different numbers of intact Cw thermal conduction pathways (a–c), and digital photographs of thermally conductive 1D-Cw/PLA composites (d–f).

thermal conduction pathways rises. For instance, when the volume fraction of Cw is 25.1 vol%, the $\lambda_{//}$ of 1D-Cw/PLA composites escalates from 2.26 to 4.23 W m^{-1} K^{-1} as the number of intact Cw thermal conduction pathways surges from 0 to 20, resulting in an enhancement of 87.2%. This enhancement can be attributed to the greater number of intact Cw thermal conduction pathways, which provide more efficient channels for heat transfer and improve thermal conductivities. Digital photographs of 1D-Cw/PLA composites, where the Cw are parallel and intersect the entire composites, are illustrated in Fig. 2d–f.

Fig. 3a presents the infrared thermal images of thermally conductive 1D-Cw/PLA composites (Group 4) arranged vertically along the *x*-axis (Fig. S1a). The average temperature at the top is depicted in Fig. 3a'. Sample 3 exhibits the most uniform surface temperature distribution, whereas the other samples display noticeable temperature differences at the breakpoints of

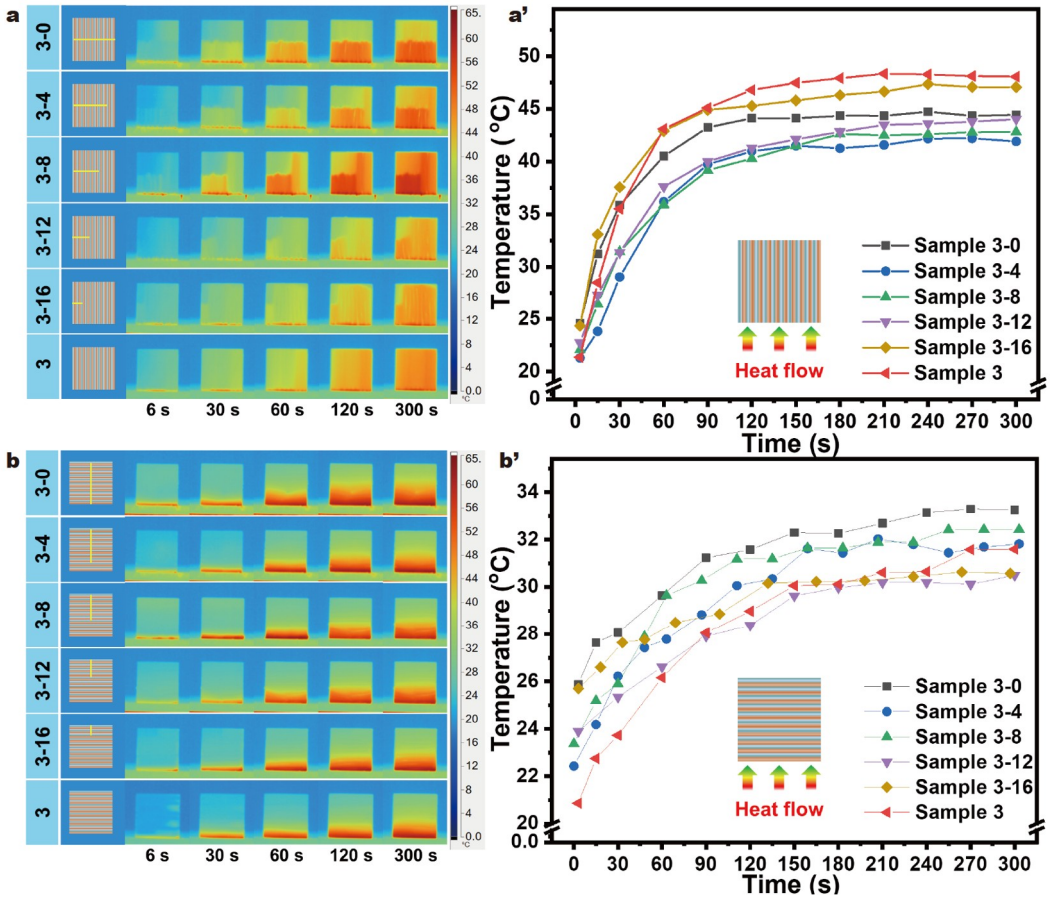

Figure 3 Infrared thermal images (a) and average temperatures at the top (a') of thermally conductive 1D-Cw/PLA composites vertically placed along the *x*-axis; infrared thermal images (b) and average temperatures at the top (b') of 1D-Cw/PLA composites vertically placed along the *y*-axis.

Cw. This discrepancy arises because the Cw thermal conduction pathways in Sample 3 remain intact, and the λ of Cw (~400 W m^{-1} K^{-1}) is significantly higher than that of the PLA matrix (~0.2 W m^{-1} K^{-1}). Consequently, heat can efficiently conduct along the Cw thermal conduction pathways and dissipate to the surroundings, resulting in a uniform temperature distribution within the samples. In contrast, 1D-Cw/PLA composites in Group 4 possess broken Cw thermal conduction pathways, leading to heat accumulation at the breakpoint and prominent temperature difference on both sides of the breakpoints. As shown in Fig. 3a', the average temperature at the top decreases with a decreasing number of intact Cw thermal conduction pathways inner 1D-Cw/PLA composites. This can be attributed to the inefficient transfer of heat across the breakpoints. Furthermore, the temperature above the breakpoints progressively decreases as the number of broken Cw thermal conduction pathways increases, resulting in a lower average temperature at the top. Fig. 3b shows the infrared thermal images of thermally conductive 1D-Cw/PLA composites (Group 4), which are vertically oriented along the *y*-axis (Fig. S1c). The corresponding average temperature at the top is depicted in Fig. 3b'. The surface temperature of all 1D-Cw/PLA composites gradually decreases along the *y*-axis, exhibiting consistent temperature distribution at the same time. This consistency arises from the similarity in the structure of 1D-Cw/PLA composites along the *y*-axis, resulting in comparable heat transfer processes. The findings highlight that a greater number of intact Cw thermal conduction pathways inner 1D-Cw/PLA composites facilitate superior thermal conduction along the pathway direction. The number of Cw thermal conduction pathways inner 1D-Cw/PLA composites significantly influences thermal conduction along the *x*-axis but has minimal impact on thermal conduction along the *y*-axis.

Length of thermal conduction pathways, the longer the better?

Fig. 4a presents the $\lambda_{//}$ of thermally conductive 1D-Cw/PLA composites containing different lengths of Cw thermal conduction pathways. The $\lambda_{//}$ of 1D-Cw/PLA composites in Group 1 (1.28, 2.28, 4.23 W m^{-1} K^{-1}) are significantly higher than those of the corresponding composites in Group 5 (1.03, 2.11, 2.99 W m^{-1} K^{-1}) and Group 6 (0.80, 1.69, 2.46 W m^{-1} K^{-1}). This discrepancy can be attributed to the fact that the 1D-Cw/PLA composites in Group 1 possess 20 intact Cw thermal conduction pathways, which enable efficient heat conduction. It is important to note that Group 5 and Group 6 both feature 2 intact Cw, with the remaining 18 Cw in Group 5 broken at the 3/4 position, while in Group 6, the broken positions are at the 1/2 position. However, when the volume fractions of Cw are the same, the $\lambda_{//}$ of Group 6 are lower than those of Group 5, indicating that longer Cw thermal conduction pathways make a greater contribution to the thermal conductivity of 1D-Cw/PLA composites. Fig. 4b depicts the infrared thermal images of thermally

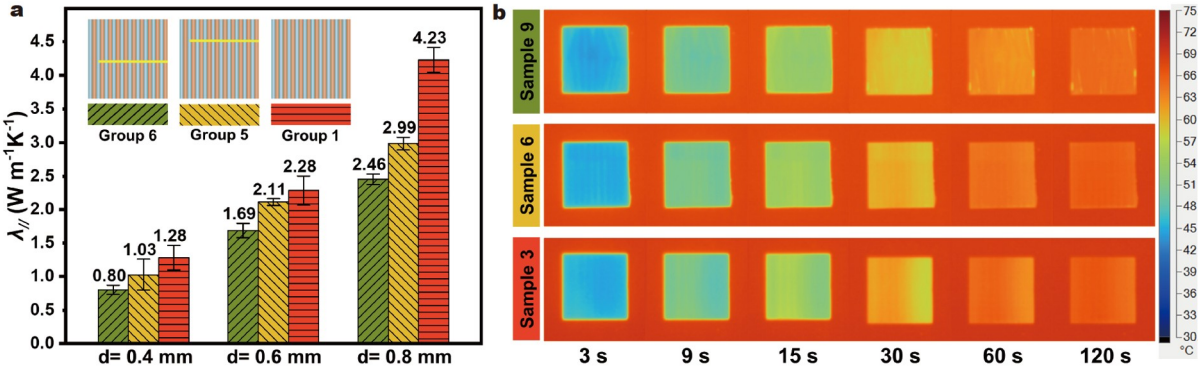

Figure 4 Influence of the length for Cw thermal conduction pathways on the $\lambda_{//}$ of thermally conductive 1D-Cw/PLA composites (a); infrared thermal images of 1D-Cw/PLA composites (b).

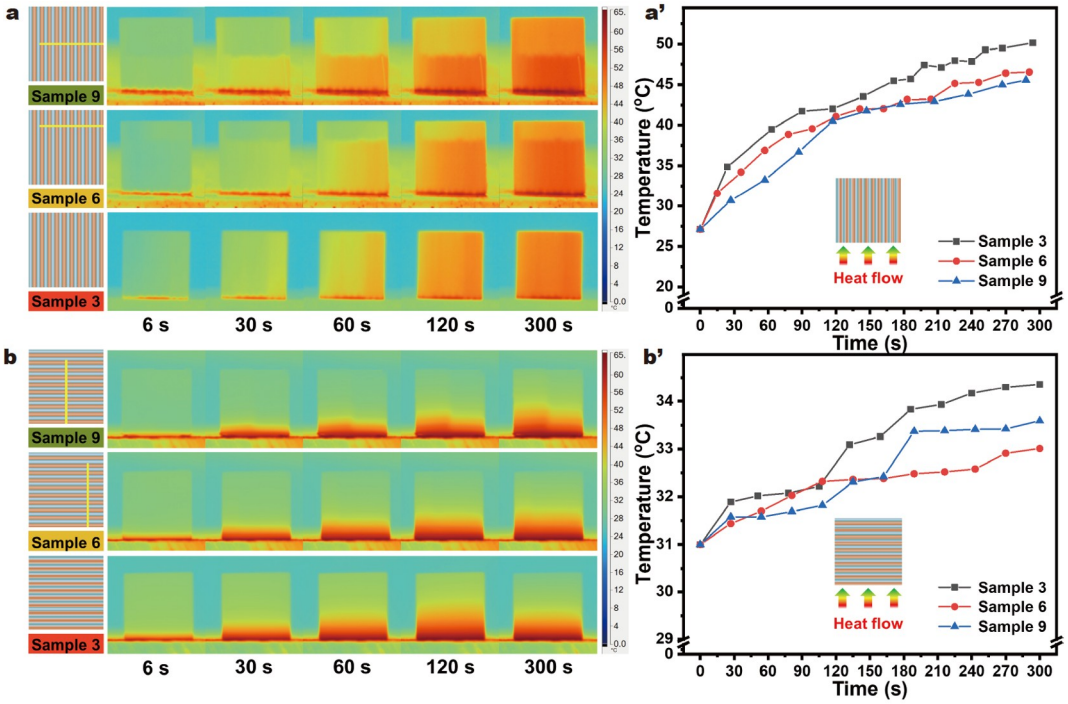

Figure 5 Infrared thermal images (a) and average temperatures at the top (a') of thermally conductive 1D-Cw/PLA composites vertically placed along the *x*-axis; infrared thermal images (b) and average temperatures at the top (b') of 1D-Cw/PLA composites vertically placed along the *y*-axis.

conductive 1D-Cw/PLA composites (with the Cw diameter of 0.8 mm and the Cw volume fraction of 25.1%), where the Cw thermal conduction pathways have different breakpoints and are horizontally placed on a heat source. The surface temperature distribution of 1D-Cw/PLA composites is uniform and increases with the duration of heating. This observation can be attributed to the fact that the position of breakpoints in the Cw thermal conduction pathways has minimal influence on the overall thermal conduction when the 1D-Cw/PLA composites are placed horizontally on the heat source. As the heating time progresses, heat accumulation increases, leading to a rise in temperature.

Fig. 5a presents the infrared thermal images of thermally conductive 1D-Cw/PLA composites (with the Cw volume fraction of 25.1% and the Cw diameter of 0.8 mm) that are vertically oriented along the *x*-axis (Fig. S1a). The average temperature at the top is displayed in Fig. 5a'. Sample 3 exhibits a relatively uniform temperature distribution without significant temperature differences. However, both Sample 6 and Sample 9 display noticeable temperature variations at the breakpoints of the Cw thermal conduction pathways. The reason behind this observation is that the Cw thermal conduction pathways in Sample 3 are all intact (Fig. S2), enabling efficient heat transfer along the *x*-axis. On the other hand, Samples 6 and 9 have broken Cw thermal conduction pathways, impeding efficient heat transfer from the bottom to the top (Fig. S2) and leading to heat accumulation at the breakpoints. Fig. 5a' illustrates the heating rate at the top of Sample 9, Sample 6, and Sample 3, which increases successively. The main contributing factor is that Sample 3, with all intact Cw thermal conduction pathways, exhibits the best thermal conduction. Additionally, Sample 6 has a more pronounced positive effect on thermal conduction along the *x*-axis

compared with Sample 9, resulting in a faster heating rate than Sample 9. Fig. 5b displays the infrared thermal images of thermally conductive 1D-Cw/PLA composites (with the Cw volume fraction of 25.1% and the Cw diameter of 0.8 mm) that are vertically oriented along the *y*-axis (Fig. S2c). The average temperature at the top is depicted in Fig. 5b'. All of the 1D-Cw/PLA composites exhibit similar temperatures, with the bottom temperature being significantly higher than the top temperature. The primary reason for this phenomenon is the absence of Cw thermal conduction pathways along the *y*-axis, which hinders efficient heat transfer and leads to substantial heat accumulation at the bottom of the composites. Fig. 5b' illustrates that the top temperature of the thermally conductive 1D-Cw/PLA composites remains relatively constant over time. This can be attributed to the structural similarity of the 1D-Cw/PLA composites along the *y*-axis, where the breakpoints of Cw thermal conduction pathways have minimal impact on heat transfer. The aforementioned results indicate that when the amount of Cw is fixed, longer Cw thermal conduction pathways inner 1D-Cw/PLA composites facilitate more effective heat conduction in the direction of the Cw pathways.

Fig. 6 shows the thermal conduction simulation of thermally conductive 1D-Cw/PLA composites. A detailed description of the simulation modeling process can be found in the Supplementary information (Fig. S3). The surface temperature of 1D-Cw/PLA composites exhibits noticeable variation along the *x*-axis, with temperatures decreasing as the distance from the heat source increases. Additionally, the temperature of the Cw inner 1D-Cw/PLA composites is significantly higher than that of the PLA matrix, and pronounced temperature differences are observed at the breakpoints of the Cw thermal conduction pathways. The main contributing factor to this phenomenon is the poor thermal conduction of PLA, resulting in substantial heat loss at the Cw-PLA interfaces during heat transfer. When the heat flows along the Cw thermal conduction pathways towards the breakpoints, maintaining efficient conduction becomes challenging, leading to prominent temperature differences on both sides of the breakpoints. Fig. 6a'–c' display the minimum temperature recorded at the top of the thermally conductive 1D-Cw/PLA composites. The obtained composites containing intact Cw thermal conduction pathways exhibit the fastest heating rate at the top, followed by composites with broken Cw thermal conduction pathways at the 3/4 position and 1/2 position, respectively. This can be attributed to the longer Cw thermal conduction pathways, which contribute more significantly to thermal conduction and result in reduced heat loss. The results of the thermal simulation emphasize that the thermal conduction of polymer composites is primarily determined by the presence of longer thermal conduction pathways. More details of the simulation process are shown in Fig. S3 and Equations S1 and S2.

Quantitative relation on thermal conduction pathways and thermal conductivities

Fig. S4 demonstrates the impact of Cw volume fraction on the $\lambda_{//}$ of thermally conductive 1D-Cw/PLA composites. The $\lambda_{//}$ of the 1D-Cw/PLA composites shows a linear increase with the volume fraction of Cw, exhibiting a strong correlation (Pearson correlation coefficient calculated using Equation S3 is 0.998). Specifically, when the volume fraction of Cw is 25.1 vol% (consisting of 20 Cw with a diameter of 0.8 mm), the $\lambda_{//}$ of 1D-Cw/PLA composites reaches 4.23 W m^{-1} K^{-1}, which corresponds to a remarkable enhancement of 1527% compared with the $\lambda_{//}$ of the pure PLA matrix (0.26 W m^{-1} K^{-1}). This significant improvement can be attributed to the substantial increase in Cw volume fraction, which significantly strengthens the dominance of parallel-mode thermal conduction (Fig. S1b). Furthermore, the series-mode thermal conduction (Fig. S1d) is also slightly enhanced (specific data can be found in Table S2), contributing to the overall enhancement in thermal conductivities of 1D-Cw/PLA composites.

In this study, one thermal conduction model (Equations (1)–(6)) has been proposed that incorporates key parameters representing the number and length of thermal conduction pathways. This model considers the impact of thermal conduction in both the *x* and *y* directions on the thermal conductivities of 1D-Cw/PLA composites. The thermal conduction in the *x* direction is greatly influenced by the number and length of Cw thermal conduction pathways, while the pathways in the *y* direction have minimal effect on heat conduction. Fig. S5a presents a schematic diagram illustrating the heat flow along the *x* direction through thermally conductive 1D-Cw/PLA composites. The equivalent thermal resistance is depicted in Fig. S5b. In this representation, R_{ai} and R_{bi} represent the thermal resistance of the a_i and b_i thermal conduction pathways, respectively. R_{pi} represents the thermal resistance at the breakpoints of thermal conduction pathways, and R_p signifies the thermal resistance of the polymer matrix. To account for the influence of the length of thermal conduction pathways on the λ_x of 1D-Cw/PLA composites, a coefficient related to the breakpoints position (σ_i) is introduced in front of the R_i term Equation (2). By utilizing Equations (1)–(6), the λ_{xy} of 1D-Cw/PLA composites were calculated, and the results are presented in Table S3. The calculated values of $\lambda_{//}/\lambda_{xy}$, which reflect the agreement between the calculated and experimental results, have an average value of 1.01. This indicates excellent prediction accuracy, as the average value is very close to 1.

$$\lambda_{xy} = \sqrt{\lambda_x \lambda_y}, \tag{1}$$

$$\lambda_x = \frac{1}{H}\sum_{i=1}^{n} \frac{1}{R_i e^{2\pi\sigma_i}(1-\sigma_i)} + \lambda_p\left(1 - \frac{n \cdot A}{H \cdot L}\right), \tag{2}$$

$$\frac{1}{\lambda_y} = \frac{1-V_f}{\lambda_p} + \frac{V_f}{\lambda_f}, \tag{3}$$

$$R_i = \frac{a_i + b_i}{\lambda_f \cdot A} + \frac{L - a_i - b_i + 0.02}{\lambda_p \cdot A}, \tag{4}$$

$$\sigma_i = \frac{a_i}{a_i + b_i + \varepsilon}, \tag{5}$$

$$A = \pi\left(\frac{D}{2}\right)^2. \tag{6}$$

In this study, a_i and b_i are derived from the matrix of thermal conduction pathways $\begin{bmatrix} a_1 & \cdots & a_n \\ b_1 & \cdots & b_n \end{bmatrix}$, where *i* ranges from 1 to *n*. Here, *n* represents the maximum number of intact thermal conduction pathways. The diameter of the 1D thermal conduction pathways is denoted by *D*. The parameter σ_i represents the position of breakpoints along the thermal conduction pathways, which can vary between 0 and 1. To avoid a zero

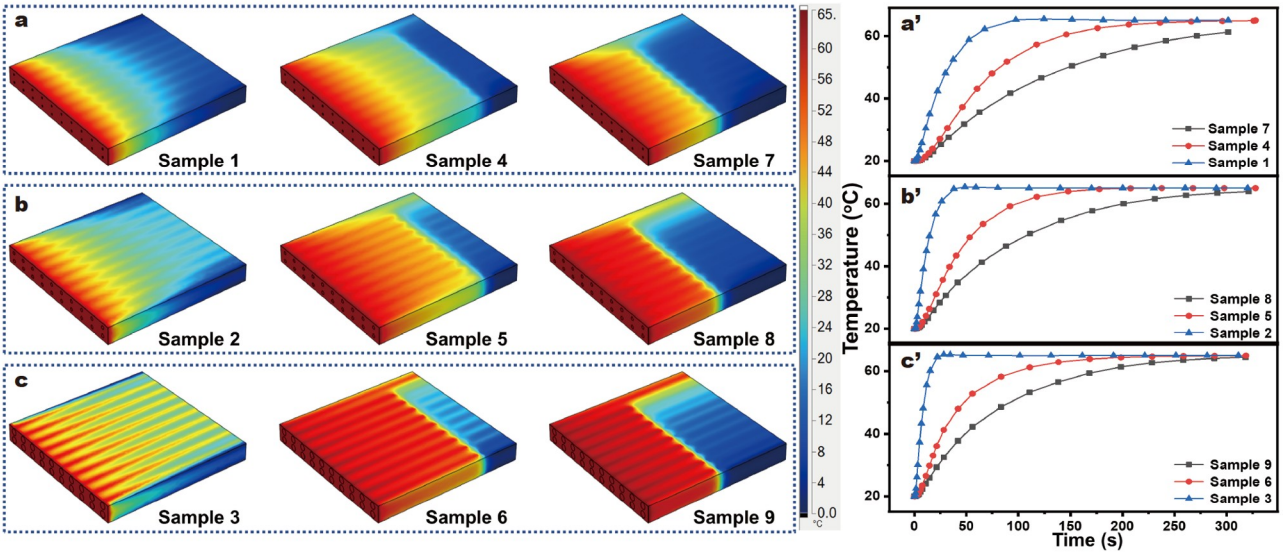

Figure 6 Finite element simulations of thermal conduction (a–c) and temperature rise (a'–c') for thermally conductive 1D-Cw/PLA composites.

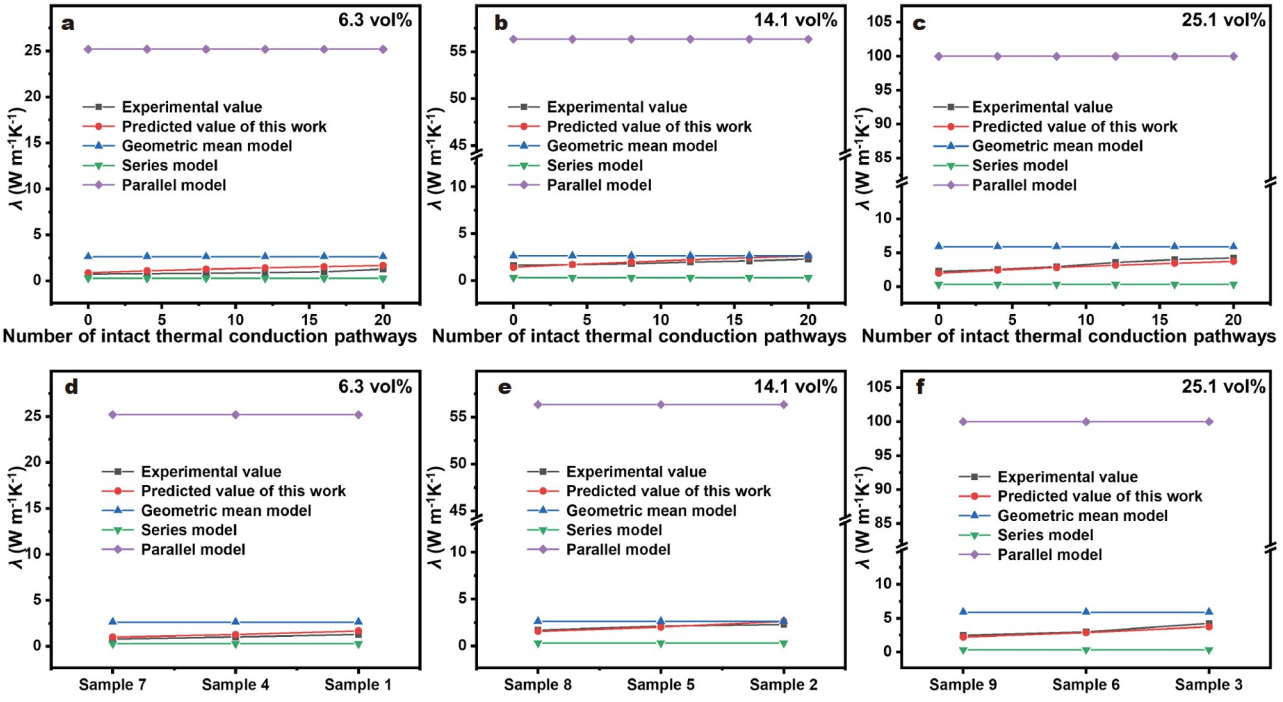

Figure 7 Comparison of the measured and predicted λ of thermally conductive 1D-Cw/PLA composites.

denominator, ε is introduced as an infinitesimal quantity. The value R_i is associated with the thermal resistance of the thermal conduction pathways. The volume fraction of thermal conduction pathways is represented by V_f. Furthermore, λ_f denotes the thermal conductivity of thermally conductive fillers, with the λ of Cw being approximately 400 W m^{-1} K^{-1}. On the other hand, λ_p corresponds to the λ of the polymer matrix, where that of PLA is 0.26 W m^{-1} K^{-1}.

Fig. 7 presents a comparison between the measured and predicted λ values for thermally conductive 1D-Cw/PLA composites. The measured λ values are higher than the predictions from the series model, but lower than the predictions from the parallel model. The predicted λ values from the geometric mean model [41,42] exhibit a certain degree of agreement with the measured values. However, our established thermal conduction model demonstrates the optimal match between the predicted and measured λ values. The primary reason for this is that the parallel model (Equation S4) [43,44] and the series model (Equation S5) [45–47] only consider heat transfer along a single direction, which fails to account for the specific thermal conduction behavior of 1D-Cw/PLA composites. Although the geometric mean model (Equation S6) incorporates heat transfer

in both the x and y directions, it does not consider the influence of thermal conduction pathway length. As a result, its predicted λ values for 1D-Cw/PLA composites still do not accurately match the actual values. In contrast, our established thermal conduction model Equations (1)–(6) considers heat transfer in both the x and y directions inner 1D-Cw/PLA composites. Additionally, it considers the lengths and numbers of thermal conduction pathways. As a result, our established thermal conduction model can accurately quantify the influence of thermal conduction pathways on the thermal conductivities.

Based on the data in Table S3, by referring to the Mann-Whitney U test (Supplementary information), it is concluded that there is no significant difference between the values of $\lambda_{//}$ and λ_{xy} at a significance level of 0.05. In other words, based on a 95% confidence level, there is no significant difference between the predicted λ values obtained from our established thermal conduction model and the actual λ values. Furthermore, Table S4 presents the λ of this work and other published work about Cu/polymer composites. It can be observed that the λ of 1D-Cw/PLA composites in this work exhibit significant advantages compared with others, which can be attributed to the optimized design of the thermal conduction pathways.

CONCLUSIONS

In summary, thermally conductive 1D-Cw/PLA composites with controllable lengths and numbers of thermal conduction pathways have been successfully prepared using the 3D printing technology. The influences of thermal conduction pathways on the thermal conductivity are thoroughly investigated, and a quantitative relationship between the above two factors is established. It is observed that the $\lambda_{//}$ of thermally conductive 1D-Cw/PLA composites is positively correlated with the numbers and lengths of Cw thermal conduction pathways, while maintaining the same amount of Cw. Specifically, when the volume fraction of Cw is 25.1 vol%, the 1D-Cw/PLA composites with 20 intact Cw thermal conduction pathways exhibit an impressive $\lambda_{//}$ of 4.23 W m^{-1} K^{-1}, which is 87.2% higher than that of composites without intact Cw thermal conduction pathways (2.26 W m^{-1} K^{-1}), 72.0% higher than that of composites with short Cw pathways (2 intact Cw and 18 broken at the half, 2.46 W m^{-1} K^{-1}), and remarkably 1527% higher than that of the pure PLA matrix (0.26 W m^{-1} K^{-1}). Furthermore, one improved thermal conduction model and an empirical equation are proposed and established, and the predicted λ values show no significant difference from the measured λ at a 95% confidence level, indicating good agreement between model prediction and the experimental results.

Received 26 May 2023; accepted 3 July 2023; published online 8 September 2023

1 Li MD, Shen XQ, Chen X, *et al.* Thermal management of chips by a device prototype using synergistic effects of 3-D heat-conductive network and electrocaloric refrigeration. Nat Commun, 2022, 13: 5849
2 Lin Y, Kang Q, Wei H, *et al.* Spider web-inspired graphene skeleton-based high thermal conductivity phase change nanocomposites for battery thermal management. Nano-Micro Lett, 2021, 13: 180
3 Chen J, Huang X, Sun B, *et al.* Highly thermally conductive yet electrically insulating polymer/boron nitride nanosheets nanocomposite films for improved thermal management capability. ACS Nano, 2019, 13: 337–345
4 Zhang H, He Q, Yu H, *et al.* A bioinspired polymer-based composite displaying both strong adhesion and anisotropic thermal conductivity. Adv Funct Mater, 2023, 33: 2211985
5 Shi X, Zhang R, Ruan K, *et al.* Improvement of thermal conductivities and simulation model for glass fabrics reinforced epoxy laminated composites *via* introducing hetero-structured BNN-30@BNNS fillers. J Mater Sci Tech, 2021, 82: 239–249
6 Kim D, Lee YJ, Ahn KH. Interconnected network of Ag and Cu in bioplastics for ultrahigh electromagnetic interference shielding efficiency with high thermal conductivity. Compos Commun, 2022, 30: 101093
7 Wang Z, Fan JF, He D, *et al.* Superior stretchable, low thermal resistance and efficient self-healing composite elastomers for thermal management. J Mater Chem A, 2022, 10: 21923–21932
8 Chen Y, Zhang H, Chen J, *et al.* Thermally conductive but electrically insulating polybenzazole nanofiber/boron nitride nanosheets nanocomposite paper for heat dissipation of 5G base stations and transformers. ACS Nano, 2022, 16: 14323–14333
9 Wang S, Wen B. Effect of functional filler morphology on the crystallization behavior and thermal conductivity of PET resin: A comparative study of three different shapes of BN as heterogeneous nucleating agents. Compos Sci Tech, 2022, 222: 109346
10 Yang S, Wang Q, Wen B. Highly thermally conductive and superior electrical insulation polymer composites *via in situ* thermal expansion of expanded graphite and *in situ* oxidation of aluminum nanoflakes. ACS Appl Mater Interfaces, 2021, 13: 1511–1523
11 Cao M, Li Z, Lu J, *et al.* Vertical array of graphite oxide liquid crystal by microwire shearing for highly thermally conductive composites. Adv Mater, 2023, 35: 2300077
12 Ruan K, Shi X, Zhang Y, *et al.* Electric-field-induced alignment of functionalized carbon nanotubes inside thermally conductive liquid crystalline polyimide composite films. Angew Chem Int Ed, 2023, 62: e202309010
13 Jiang J, Yang S, Li L, *et al.* High thermal conductivity polylactic acid composite for 3D printing: Synergistic effect of graphene and alumina. Polym Adv Technol, 2020, 31: 1291–1299
14 Barani Z, Mohammadzadeh A, Geremew A, *et al.* Thermal properties of the binary-filler hybrid composites with graphene and copper nanoparticles. Adv Funct Mater, 2020, 30: 1904008
15 Han G, Cheng H, He C, *et al.* Silver nanoparticles bridging segregated hexagonal boron nitride networks for enhancing the thermal conductivity of polystyrene composites. Compos Commun, 2022, 34: 101267
16 Dehdari Ebrahimi N, Ju YS. Thermal conductivity of sintered copper samples prepared using 3D printing-compatible polymer composite filaments. Additive Manufact, 2018, 24: 479–485
17 Yang S, Li W, Bai S, *et al.* Fabrication of morphologically controlled composites with high thermal conductivity and dielectric performance from aluminum nanoflake and recycled plastic package. ACS Appl Mater Interfaces, 2019, 11: 3388–3399
18 Lule Z, Kim J. Thermally conductive and highly rigid polylactic acid (PLA) hybrid composite filled with surface treated alumina/nano-sized aluminum nitride. Compos Part A-Appl Sci Manufact, 2019, 124: 105506
19 Wang Y, Jin H, Shen J, *et al.* Thermally conductive poly(lactic acid)/boron nitride composites *via* regenerated cellulose assisted Pickering emulsion approach. J Mater Sci Tech, 2022, 101: 146–154
20 Lee W, Kim J. Highly thermal conductive and electrical insulating epoxy composites with a three-dimensional filler network by sintering silver nanowires on aluminum nitride surface. Polymers, 2021, 13: 694
21 Han Y, Ruan K, Gu J. Multifunctional thermally conductive composite films based on fungal tree-like heterostructured silver nanowires@boron nitride nanosheets and aramid nanofibers. Angew Chem Int Ed, 2023, 62: e202216093
22 Zhang X, Li J, Gao Q, *et al.* Nerve-fiber-inspired construction of 3D graphene "tracks" supported by wood fibers for multifunctional biocomposite with metal-level thermal conductivity. Adv Funct Mater, 2023, 33: 2213274
23 Huang R, Ding D, Guo X, *et al.* Improving through-plane thermal conductivity of PDMS-based composites using highly oriented carbon

fibers bridged by Al_2O_3 particles. Compos Sci Tech, 2022, 230: 109717
24 Chen S, Seveno D, Gorbatikh L. Multiscale modeling and maximizing the thermal conductivity of polyamide-6 reinforced by highly entangled graphene flakes. Compos Part A-Appl Sci Manufact, 2021, 151: 106632
25 Qian X, Zhou J, Chen G. Phonon-engineered extreme thermal conductivity materials. Nat Mater, 2021, 20: 1188–1202
26 Zheng H, Xu G, Wu K, *et al.* Highly intrinsic thermally conductive electrospinning film with intermolecular interaction. J Phys Chem C, 2021, 125: 21580–21587
27 Cao H, Li Y, Xu W, *et al.* Leakage-proof flexible phase change gels with salient thermal conductivity for efficient thermal management. ACS Appl Mater Interfaces, 2022, 14: 52411–52421
28 Zhang Y, Ruan K, Zhou K, *et al.* Controlled distributed $Ti_3C_2T_x$ hollow microspheres on thermally conductive polyimide composite films for excellent electromagnetic interference shielding. Adv Mater, 2023, 35: 2211642
29 Sun D, Gu T, Mao Y, *et al.* Fabricating high-thermal-conductivity, high-strength, and high-toughness polylactic acid-based blend composites *via* constructing multioriented microstructures. Biomacromolecules, 2022, 23: 1789–1802
30 Ma TB, Ma H, Ruan KP, *et al.* Thermally conductive poly(lactic acid) composites with superior electromagnetic shielding performances *via* 3D printing technology. Chin J Polym Sci, 2022, 40: 248–255
31 He X, Ou D, Wu S, *et al.* A mini review on factors affecting network in thermally enhanced polymer composites: Filler content, shape, size, and tailoring methods. Adv Compos Hybrid Mater, 2022, 5: 21–38
32 Zhao C, Li Y, Liu Y, *et al.* A critical review of the preparation strategies of thermally conductive and electrically insulating polymeric materials and their applications in heat dissipation of electronic devices. Adv Compos Hybrid Mater, 2023, 6: 27
33 Agari Y, Ueda A, Nagai S. Thermal conductivity of a polyethylene filled with disoriented short-cut carbon fibers. J Appl Polym Sci, 1991, 43: 1117–1124
34 Hao M, Qian X, Zhang Y, *et al.* Thermal conductivity enhancement of carbon fiber/epoxy composites *via* constructing three-dimensionally aligned hybrid thermal conductive structures on fiber surfaces. Compos Sci Tech, 2023, 231: 109800
35 Privalko VP, Novikov VV(eds.). Thermal and Electrical Conductivity of Polymer Materials. Berlin & Heidelberg: Springer Berlin Heidelberg, 1995
36 Long Y, Zhang Z, Yan C, *et al.* Multi-objective optimization for improving printing efficiency and mechanical properties of 3D-printed continuous plant fibre composites. Compos Commun, 2022, 35: 101283
37 Guo H, Zhao H, Niu H, *et al.* Highly thermally conductive 3D printed graphene filled polymer composites for scalable thermal management applications. ACS Nano, 2021, 15: 6917–6928
38 Huttunen E, Nykänen MT, Alexandersen J. Material extrusion additive manufacturing and experimental testing of topology-optimised passive heat sinks using a thermally-conductive plastic filament. Additive Manufact, 2022, 59: 103123
39 Gao J, Hao M, Wang Y, *et al.* 3D printing boron nitride nanosheets filled thermoplastic polyurethane composites with enhanced mechanical and thermal conductive properties. Additive Manufact, 2022, 56: 102897
40 Guiney LM, Mansukhani ND, Jakus AE, *et al.* Three-dimensional printing of cytocompatible, thermally conductive hexagonal boron nitride nanocomposites. Nano Lett, 2018, 18: 3488–3493
41 Taleb O, Barzycki DC, Polanco CG, *et al.* Assessing effective medium theories for conduction through lamellar composites. Int J Heat Mass Transfer, 2022, 188: 122631
42 Chaudhary DR, Bhandari RC. Heat transfer through a three-phase porous medium. J Phys D-Appl Phys, 1968, 1: 815–817
43 Cai Y, Yu H, Chen C, *et al.* Improved thermal conductivities of vertically aligned carbon nanotube arrays using three-dimensional carbon nanotube networks. Carbon, 2022, 196: 902–912
44 Peng H, Huang J, Ren H, *et al.* Parallel structure enhanced polysilylarylenyne/$Ca_{0.9}La_{0.067}TiO_3$ composites with ultra-high dielectric constant and thermal conductivity. ACS Appl Mater Interfaces, 2022, 14: 45893–45903
45 Potenza M, Petracci I, Corasaniti S. Transient thermal behaviour of high thermal conductivity graphene based composite materials: Experiments and theoretical models. Int J Thermal Sci, 2023, 188: 108253
46 Losego MD, Blitz IP, Vaia RA, *et al.* Ultralow thermal conductivity in organoclay nanolaminates synthesized *via* simple self-assembly. Nano Lett, 2013, 13: 2215–2219
47 Zhao S, Zhu R, Fu Y. Piezothermic transduction of functional composite materials. ACS Appl Mater Interfaces, 2019, 11: 4588–4596

Acknowledgements This work was supported by the National Natural Science Foundation of China (51973173), the Technological Base Scientific Research Projects (Highly Thermal conductivity Nonmetal Materials), and the Fundamental Research Funds for the Central Universities. Ruan K would like to thank the Innovation Foundation for Doctor Dissertation of Northwestern Polytechnical University (CX2022073). This work was also financially supported by the Polymer Electromagnetic Functional Materials Innovation Team of Shaanxi Sanqin Scholars.

Author contributions Gu J and Ma T designed the samples; Ma T and Guo Y performed the experiments; Ma T, Ruan K and Han Y performed the data analysis; Ma T and Ruan K wrote the paper with support from Gu J. All authors contributed to the general discussion.

Conflict of interest The authors declare that they have no conflict of interest.

Supplementary information Supporting data are available in the online version of the paper.

Tengbo Ma obtained his Bachelor degree from Northwestern Polytechnical University in 2016. Currently he is a PhD candidate majoring in materials science at Northwestern Polytechnical University. His research interests include structural optimization, performance improvement, and mechanism research of thermally conductive polymer composites.

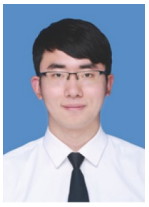

Kunpeng Ruan obtained his Bachelor degree from Northwestern Polytechnical University in 2019. Currently he is a PhD candidate majoring in materials science at Northwestern Polytechnical University. His research interests include structural optimization, performance improvement and mechanism investigation of intrinsically thermally conductive polyimide and its composite films.

Yongqiang Guo obtained his PhD degree from Northwestern Polytechnical University in 2022. Currently he is a postdoc at Beihang University. His research interests focus on structural optimization, performance improvement and mechanism investigation of thermally conductive polymer composites.

Junwei Gu received his PhD degree from Northwestern Polytechnical University, China in 2010. He is a professor at the School of Chemistry and Chemical Engineering, Northwestern Polytechnical University. His research interests include thermally conductive polymers and composites, fiber-reinforced polymer matrix wave-transparent composites, and electromagnetic interference shielding polymer matrix composites.

3D打印调控铜线/聚乳酸复合材料的导热通路长度和数量

马腾博[1†], 阮坤鹏[1†], 郭永强[2*], 韩懿鑫[1], 顾军渭[1*]

摘要 导热通路对理解导热高分子复合材料的导热行为至关重要，但目前有关导热通路属性(长度、数量)对高分子复合材料导热系数的影响机制缺乏深入研究．本文采用3D打印技术制备了铜线(Cw)导热通路长度和数量可控的一维铜线/聚乳酸(1D-Cw/PLA)导热复合材料，建立了针对一维导热通路的高分子复合材料的导热模型，明晰了其导热通路属性与其导热性能的定量关系．相同Cw用量下，1D-Cw/PLA导热复合材料的面内导热系数与导热通路的数量和长度呈正相关．采用本文构建的导热模型和经验方程对1D-Cw/PLA复合材料的导热系数进行预测，95%的置信度表明预测值与实测值无显著差异.